Genomics Proteomics Bioinformatics 20 (2022) 597–613

Genomics Proteomics Bioinformatics

www.elsevier.com/locate/gpb
www.sciencedirect.com

ORIGINAL RESEARCH

Phosphoproteomics Reveals the AMPK Substrate Network in Response to DNA Damage and Histone Acetylation

Yuejing Jiang [1,3,#], Xiaoji Cong [2,3,#], Shangwen Jiang [2,3], Ying Dong [1,3], Lei Zhao [2], Yi Zang [1,*], Minjia Tan [2,*], Jia Li [1,4,*]

[1] *National Center for Drug Screening, State Key Laboratory of Drug Research, Shanghai Institute of Materia Medica, Chinese Academy of Sciences, Shanghai 201203, China*
[2] *Chemical Proteomics Center, State Key Laboratory of Drug Research, Shanghai Institute of Materia Medica, Chinese Academy of Sciences, Shanghai 201203, China*
[3] *University of Chinese Academy of Sciences, Beijing 100049, China*
[4] *Open Studio for Druggability Research of Marine Natural Products, Pilot National Laboratory for Marine Science and Technology (Qingdao), Qingdao 266237, China*

Received 2 July 2019; revised 12 August 2020; accepted 11 November 2020
Available online 17 February 2021

Handled by Kyle Biggar

KEYWORDS

AMPK;
Phosphoproteomics;
Histone modification;
DNA damage;
Apoptosis

Abstract AMP-activated protein kinase (**AMPK**) is a conserved energy sensor that plays roles in diverse biological processes via phosphorylating various substrates. Emerging studies have demonstrated the regulatory roles of AMPK in DNA repair, but the underlying mechanisms remain to be fully understood. Herein, using mass spectrometry-based proteomic technologies, we systematically investigate the regulatory network of AMPK in DNA damage response (DDR). Our system-wide phosphoproteome study uncovers a variety of newly-identified potential substrates involved in diverse biological processes, whereas our system-wide **histone modification** analysis reveals a link between AMPK and histone acetylation. Together with these findings, we discover that AMPK promotes **apoptosis** by phosphorylating apoptosis-stimulating of p53 protein 2 (ASPP2) in an irradiation (IR)-dependent manner and regulates histone acetylation by phosphorylating histone deacetylase 9 (HDAC9) in an IR-independent manner. Besides, we reveal that disrupting the histone acetylation by the bromodomain BRD4 inhibitor JQ-1 enhances the sensitivity of AMPK-deficient cells to IR. Therefore, our study has provided a resource to investigate the interplay

* Corresponding authors.
E-mail: yzang@simm.ac.cn (Zang Y), mjtan@simm.ac.cn (Tan M), jli@simm.ac.cn (Li J).
# Equal contribution.

Peer review under responsibility of Beijing Institute of Genomics, Chinese Academy of Sciences / China National Center for Bioinformation and Genetics Society of China.

https://doi.org/10.1016/j.gpb.2020.09.003

between phosphorylation and histone acetylation underlying the regulatory network of AMPK, which could be beneficial to understand the exact role of AMPK in DDR.

Introduction

AMP-activated protein kinase (AMPK) is a heterotrimeric serine/threonine kinase complex with one catalytic subunit α (including α1 and α2) and two regulatory subunits β (including β1 and β2) and γ (including γ1, γ2, and γ3), which contains theoretically 12 different types of heterotrimers. As a central metabolic sensor to restore intercellular energy homeostasis, activation of AMPK switches off anabolic pathways that consume ATP and switches on catabolic pathways that generate ATP. There are two coordinated mechanisms that modulate the activity of AMPK. One is phosphorylation at its conserved Thr172 in the activation loop of AMPKα1 subunit, which is regulated by upstream kinases liver kinase B1 (LKB1) and calmodulin-dependent protein kinase kinase β (CaMKKβ). The other is the binding of ADP/AMP to γ subunit to allosterically activate AMPK by stabilizing it in an active conformation [1]. Once activated, AMPK, in turn, further phosphorylates diverse downstream substrates, such as metabolic enzymes, transcription factors, and co-activators, to balance energy homeostasis either by short-term provocations of metabolic signaling cascades or by long-term regulations of transcription and posttranslational modification [2].

Emerging studies have uncovered the contradictory roles of AMPK in tumor development and cancer therapy. AMPK was reported to be a key mediator contributing to the suppression effect of LKB1 signaling cascades [3,4]. Such a hypothesis is supported by a series of studies from metformin, whose mechanism of action is widely recognized to be associated with AMPK activation [5,6]. Metformin could significantly inhibit tumor growth and improve chemo-sensitivity and radiosensitivity via AMPK activation in various types of tumors [7–10]. Remarkably, several studies showed the effect of metformin to kill the cancer stem-like cells [11–13], which are considered a major barrier in cancer therapy. Studies from another AMPK activator 5-aminoimidazole-4-carboxamide-1-β-D-ribofuranoside (AICAR) [14] also supported such a hypothesis. One the other hand, other studies suggest that AMPK could be a context-dependent tumor promoter. The biological consequences in which AMPK is supra-physiologically activated by compounds are different from those in which AMPK is physiologically activated by cellular stresses [15]. Indeed, the AMPK energy-sensing pathway supports cells to survive in hypoxic and nutrient-deficient conditions, which is regarded as a typical tumor microenvironment. Supporting such an assumption is that autophagy, which is partially considered to be regulated by AMPK, might provide enough nutrients to support cancer survival by degrading cellular organelles or proteins [16]. In addition, glyceraldehyde-3-phosphate dehydrogenase (GAPDH) generated by fatty acid oxidation, which is up-regulated by AMPK activation, is beneficial to protect cancer cells from oxidative stresses by neutralizing cytotoxic reactive oxygen species (ROS) [17]. Furthermore, increasing phospho-AMPK levels is associated with higher tumor grade in prostate cancer [18]. Therefore, these contradictory findings suggest an urgent need to understand the exact role of AMPK in tumor biology.

The aforementioned puzzling phenomenon could be partially explained by the complicated functional consequences caused by the diverse substrates of AMPK. For example, AMPK-mediated phosphorylation on p53 [19–21] and the mechanistic target of rapamycin complex 1 (mTORC1) [22–24] signaling pathway are essential for activator-induced tumor suppression. In contrast, AMPK could promote tumor growth via other mechanisms, including the induction of mitophagy by phosphorylating ULK1 [16], the up-regulation of stress-induced gene transcription by phosphorylating histone H2B [25], and the promotion of FA oxidation to neutralize oxidative stress [17]. Moreover, new substrates identified in mitochondrial fission [26,27], hippo-YAP signaling pathway [28], and mitosis [22] implied a subtle regulatory role of AMPK in cancer. In addition, the pharmacological effects of two anti-cancer drugs, etoposide and cisplatin, were reported to be partially dependent on AMPK activation [29–31]. Despite these understanding, the detailed mechanism is not yet fully understood how AMPK coordinately regulates these cascades and whether some unknown partners are involved in this process. Indeed, our knowledge of the cancer-associated AMPK substrates is still limited. Therefore, a comprehensive understanding of the substrates of AMPK is a critical step toward understanding the role of AMPK in cancer.

Human tumors share various biological hallmarks acquired during multistep development. One of these hallmarks is genome instability, which is acquired during cancer development and drug resistance [32]. Abnormal or deficient DNA damage response (DDR) results in genomic instability and neoplastic transformation. In recent years, emerging reports suggested that AMPK was involved in DDR, but the regulatory role remained to be fully understood [33–35].

To address this question, we carried out a system-wide phosphoproteome study by mass spectrometry (MS)-based proteomic technologies. Our results showed that a variety of newly-identified substrates were involved in diverse biological activities, which shed light on a broad and complex regulatory network of AMPK in DDR. In addition, our system-wide histone modification analysis showed that AMPK played a role in modulating global histone acetylation levels. Disrupting the histone acetylation by the bromodomain BRD4 inhibitor JQ-1 enhanced the sensitivity of AMPK-deficient cells to irradiation (IR) via induction of apoptosis. Thus, our study provided an abundant resource to investigate the interplay between phosphorylation and histone acetylation underlying the regulatory network of AMPK, which might be beneficial to understand the exact role of AMPK in tumor biology.

Results

Establishment of AMPKα1/α2-double knockout cell lines by TALENs

We first investigated whether AMPK was involved in DDR. X-ray IR induced cellular DNA damages and activated DDR signaling to repair DNA double strand breaks (DSBs).

After a single dose of X-ray IR exposure, both AMPK activation signal phospho-AMPK (Thr172) and its substrate signal phospho-ACC (Thr79) increased as IR dose elevated, suggesting that AMPK was activated in a dose-dependent way in DDR (**Figure 1**A and B). To investigate the underlying mechanisms of AMPK activation during DDR, we established stable AMPKα1/α2 (two AMPK catalytic isoforms)-double knockout (KO) mouse embryonic fibroblast (MEF) cell lines using Transcription Activator-Like Effector Nuclease (TALEN) technology. TALEN technology is a genome-editing method widely used to generate KO *Caenorhabditis elegans*, rats, mice, and zebrafishes [36–42]. It is also used in genomic modification of human embryonic stem cells and induced pluripotent stem cells (iPSCs). The establishment method was according to previous reports [39,41,43]. We obtained three stable AMPKα1/α2-KO cell lines (named as 1#, 2#, and 3#). The AMPKα1 and α2 protein expression levels could not be detected by immunoblot, suggesting successful deletion of total AMPKα subunits (Figure 1C). To evaluate whether downstream signaling was also impaired, we treated cells with AMPK activator AICAR. In contrast to wild-type (WT) MEF cells, AICAR treatment did not induce AMPK activation signal phospho-AMPKα (Thr172) and substrate signal phospho-ACC (Thr79) in the three KO cell lines, further suggesting the loss of AMPKα1 and α2 kinase activity (Figure 1C). Besides, we extracted genomic DNA from individual cell lines for sequencing and found nucleotide deletion in leading chain and lagging chain. In addition, our genomic sequencing of these cell lines also showed that nucleotide deletion happened in both leading chain and lagging chain in all three cell lines (Figure S1). In contrast to 3# cell line, TALENs induced non-3 nt-deletion in 1# and 2# cell lines that resulted in absolute target KO in genomic level because of coding frame shift. We next chose 1# and 2# cell lines for further functional assay. To address the issue whether AMPK is involved in DDR, we exposed WT MEF, 1#, and 2# cells to a single dose of X-ray IR. We observed an increasing γH2A.X (phospho-H2A.X Ser139) foci (a marker of DSB measured by immunofluorescence) after IR exposure (Figure 1D and E). Comparable percentage of γH2A.X foci-positive cells at 48 h post-IR in 1# and 2# cell lines suggested that these two cell lines could be functionally equivalent in DDR. Therefore, 1# cell line (defined as AMPKα-KO cells in this study) was selected for further proteome analysis. Meanwhile, compared with WT MEFs, more γH2A.X foci remained at 48 h in 1# and 2# cell lines, suggesting that AMPKα was required to promote DSB repair efficiency. Besides, a prolonged G2 phase arrest was observed in AMPKα-KO cells after IR (WT, 0 h 27.30% to 24 h 25.72%, $P = 0.690$; KO, 0 h 30.55% to 24 h 40.65%, $P = 0.011$) (Figure 1F and G). Taken together, these results suggested that the kinase activity of AMPKα is required in DDR, but the underlying regulatory network remains to be understood.

Quantitative phosphoproteomics uncovered broad signaling pathways regulated by AMPK in DDR

To further profile the regulatory networks of AMPK in DDR, we carried out a system-wide phosphoproteome analysis (**Figure 2**A). Previous studies suggested that more abundant signaling pathways would be activated in response to IR at relatively high doses than at low doses [44,45]. According to the result that AMPK activated and phosphorylated substrates in a dose-dependent manner (Figure 1A and B), we hypothesized that AMPK likely activated more signaling pathways at higher IR doses. Therefore, a relatively high dose (10 Gy) that mimicked the stressed cellular microenvironment in radio-combined cancer therapy was selected in further experiment. The proteome of AMPKα-KO cells was labeled with "heavy" ($^{13}C_6$-Lys and $^{13}C_6^{15}N_4$-Arg) amino acids, whereas the proteome of the WT cells was labeled with "light" ($^{12}C_6$-Lys and $^{12}C_6^{14}N_4$-Arg) amino acids in cell culture. WT and AMPKα-KO cells were prepared in both basal group and IR group at the same time. After IR, cells from IR group were released for 90 min before harvest to fully activate diverse signaling pathways involved in DDR. Proteins were extracted from the two cell populations and mixed equally for further analysis. Two types of proteases, trypsin and chymotrypsin, were used to improve the sequence coverage of the phosphoproteome as previously reported [46]. Collectively, we identified 11,065 phosphosites with a localization probability higher than 0.75 in the basal and IR groups. First, we verified the reproducibility between replicate experiments in basal (trypsin and chymotrypsin digested) and IR (trypsin and chymotrypsin digested) groups (Figure S2). Scatter plot depicting the correlation between two replicates in each group showed high correlation coefficient values (r = 0.78–0.84), suggesting reliable reproducibility of our phosphoproteomic data. We used a criterion of more than 1.5-fold between basal and IR groups to define those significantly different phosphosites ($P < 0.05$ by Student's *t*-test). A total of 539 down-regulated phosphosites and 389 up-regulated phosphosites were identified in the basal group (Figure 2B; Table S1). Phosphosites of well-known AMPK substrates were found to be significantly down-regulated in AMPKα-KO cells (Figure 2B). Motif analysis showed that the consensus AMPK substrate motif could be enriched in the down-regulated phosphosites in AMPKα-KO cells (Figure S3). Together, these results suggested the high quality of our proteomic data.

Meanwhile, 1216 down-regulated phosphosites and 169 up-regulated phosphosites were identified in the IR group (Figure 2C and D; Table S1). This result indicated that various protein phosphorylation events could be regulated by AMPK during DDR. Of these significantly down-regulated phosphosites, 471 phosphosites (38%) were also down-regulated (FC < 0.667) in the basal group (Figure 2B). In contrast, 257 phosphosites (21%) remained unchanged (0.8 < FC < 1.2) in the basal group (Figure 2B and D). For example, phosphorylation on Xrcc1 Thr452 was slightly down-regulated in the basal group ($\log_2$ FC = –0.28, $P = 0.01$), while it was significantly altered after IR ($\log_2$ FC = –0.78, $P = 0.005$). Therefore, these results suggested that AMPK played additional regulatory roles when cells suffered severe genomic stress, as compared to its routine regulatory roles in basal status.

To gain insight into the possible biological functions of AMPK during DDR, we subjected all significantly down-regulated and up-regulated phosphoproteins identified in IR group to bioinformatic enrichment analysis using GO and KEGG databases by the DAVID bioinformatic tool. In consistent with a prolonged G2 phase arrest observed in AMPKα-KO cells after IR (Figure 1F and G), we discovered that the changed phosphoproteins were significantly enriched in DNA damage repair-associated events, such as cell cycle,

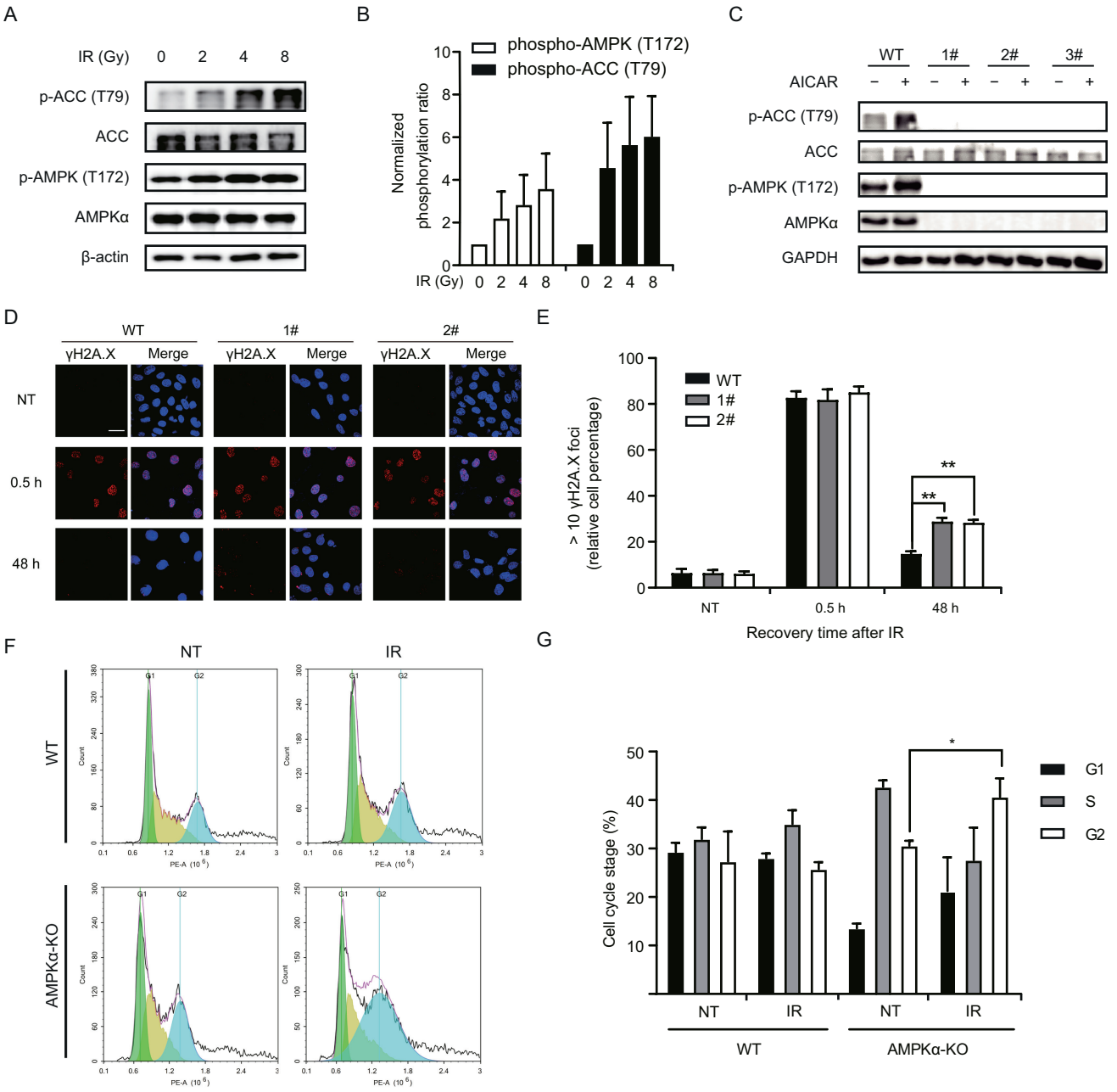

Figure 1 AMPK plays protective roles in DDR

A. IR induces AMPK activation in a dose-dependent manner. The WT MEF cells were exposed to increasing does of X-ray (0, 2, 4, and 8 Gy) and sampled at 10 min after IR. **B.** Quantitative result of (A) is measured by ImageJ software. Data are shown as mean ± SEM from three independent experiments. **C.** Validation of AMPKα1/α2-KO MEF cell lines 1#, 2#, and 3#. Parental WT MEF cells and three AMPKα1/α2 double-KO cell lines were treated with or without 1 mM AICAR for 30 min. AICAR is an AMPK activator. **D.** AMPKα1/α2 KO impairs efficient repair. The WT MEF cells and AMPKα1/α2-KO MEF cell lines 1# and 2# were exposed to a single dose of 4 Gy X-ray. After recovery for 0.5 h or 48 h, the cells were fixed and stained with anti-γH2A.X antibody and observed under microscopy. Scale bar, 40 μm. **E.** Quantitative result represented for (D). Cells with more than ten γH2A.X foci were regarded as positive ones. More than 100 cells in each group were imaged and counted. Data are analyzed with two-way ANOVA followed by Fisher's LSD tests with two-tailed distribution using GraphPad Prism software. Data are shown as mean ± SEM from two independent experiments. **, $P < 0.01$. **F.** AMPKα1/α2 KO prolongs G2 phase arrest. The WT MEF cells and AMPKα1/α2-KO MEF cell line 1# (AMPKα-KO) were treated with or without 10 Gy X-ray and cultured for 24 h before assay. **G.** Quantitative results represented for (F). Data are analyzed with two-way ANOVA followed by Fisher's LSD tests with two-tailed distribution using GraphPad Prism software. Data are shown as mean ± SEM from three independent experiments. *, $P < 0.05$. AMPK, AMP-activated protein kinase; DDR, DNA damage response; IR, irradiation; WT, wild-type; MEF, mouse embryonic fibroblast; AICAR, 5-aminoimidazole-4-carboxamide-1-β-D-ribofuranoside.

DNA repair, and transcription (Figure 2E). Surprisingly, chromatin-associated functions were also highly enriched, such as chromatin regulation and histone modification (including deacetylation, ubiquitination, and methylation), suggesting a potential regulatory role of AMPK in epigenetic modification. Meanwhile, we also discovered a potential crosstalk between DNA damage and RNA processing (both mRNA processing and rRNA processing), in consistent with emerging evidence that mRNA processing factors are involved in DNA damage signal transduction. Theoretically, BCLAF1 was assembled at damage sites via interacting with core spliceosome components while THRAP3 was excluded from damage sites as a consequence of transcription repression [47]. Phosphorylation event was one of factors to regulate the assemble and dissemble processes. The significantly up-regulated phosphosites Ser248 and Ser572 on THRAP3, as well as the significantly down-regulated phosphosite Ser284 on BCLAF1, were observed. Besides, mRNA splicing factor hnRNPUL1, a DNA-end resection regulator, was found to be significantly down-regulated at Ser4 during DDR (Figure 2F). These findings implied that the phosphorylation events on these mRNA splicing factors might be involved in DSB repair. Taken together, bioinformatic enrichment analysis revealed a broad and complicated regulatory role of AMPK involved in diverse signaling pathways.

Bioinformatic analysis identifies ASPP2 as a new substrate of AMPK involved in apoptosis

We next analyzed the significantly changed phosphoproteins in IR group by Motif-X algorithm to predict the preferred motif sequences. It was well established that AMPK phosphorylated diverse substrates at a consensus amino acid sequence motif. Briefly, –5 site and +4 site contained a hydrophobic amino acid like L/M/V/I/F (Φ), while –3 or –4 site contained at least one basic amino acid R/K (β) [48]. Motif enrichment analysis of down-regulated phosphosites in IR group was carried out. Among several enriched motifs proposed by Motif-X algorithm (**Figure 3**A), the sequences ranked 2nd and 3rd, xxxxRRxSxxxxxxx and xxxxRxxSxxxxxxx, partially matched to the classical AMPK substrate motif ΦxβxxSxxxΦ. This possibly indicated that there existed some potential AMPK substrates not strictly match the classical motif very well.

Among the aforementioned significantly down-regulated phosphosites, we further divided them into two groups, IR-independent substrates and IR-dependent substrates. The IR-dependent substrates (DNA damage-associated substrates) were phosphorylated by AMPK under DDR. These phosphosites were down-regulated in IR group but remained nearly unchanged in basal group (normalized heavy/light ratio, $0 < IR/Basal < 0.8$ and $0.8 < Basal < 1.2$). In contrast, the IR-independent substrates (general substrate candidates) were phosphorylated by AMPK independent of DDR. These phosphosites were significantly down-regulated in either basal group or IR group (heavy/light ratio < 0.67). To identify direct potential substrates of AMPK, we aligned these phosphosites in both IR-dependent and IR-independent substrates to the AMPK consensus motif. Based upon the criteria, we totally obtained 42 potential substrates (Figure 3B; **Table 1**).

To further confirm the reliability of our results, we randomly selected one of the substrates, apoptosis-stimulating of p53 protein 2 (ASPP2) for further validation. Ser479 on ASPP2 was considered as a DNA damage-associated substrate because the normalized IR/basal ratio of Ser479 on ASPP2 was 0.78 (normalized heavy/light ratio, Basal = 0.95, IR = 0.74). p53 was a well-established tumor suppressor involved in both cell cycle arrest and apoptosis. ASPP2 was initially identified as a binding partner of p53 and required in p53-mediated apoptosis [49,50]. We first investigated whether protein interaction existed between AMPK and ASPP2. Plasmids were synchronically introduced into 293T cells to overexpress Flag-ASPP2 and Myc-AMPKβ1 for 48 h, and the whole cell lysates were harvested for exogenous immunoprecipitation (IP) with the anti-Flag antibody. Immunoblot showed interaction between AMPKβ1 and ASPP2 (Figure S4). The endogenous protein–protein interaction was further confirmed in 293T cells in IP assay using AMPKβ1 antibody (Figure 3C). Bioinformatic analysis revealed that the amino acid sequence surrounding Ser479 on ASPP2 matched the AMPK substrate motif and kept conserved during species evolution (Figure 3D). Therefore, we investigated whether AMPK could phosphorylate ASPP2 at Ser479 by *in vitro* kinase assay using [^{32}P]-labeled ATP. Truncated ASPP2-(1-765 aa)-WT and mutant ASPP2-(1-765 aa)-S479A (serine converted to non-phosphorylatable alanine) that mimicked phosphonull status were purified from *Escherichia coli* and incubated with AMPKα2β2γ2 complex in kinase reaction buffer for 1 h. AMPKα2β2γ2 complex with no kinase activity was purified from *E. coli*. but retained catalytic activity after incubation with upstream kinase CAMKKβ. Robust [^{32}P] signal was induced by activated-AMPKα2β2γ2 complex on truncated ASPP2-(1-765 aa)-WT but strongly attenuated on mutant ASPP2-(1-765 aa)-S479A, suggesting that AMPK phosphorylated ASPP2 dominantly at Ser479 (Figure 3E). However, weak [^{32}P] signal detected on mutant ASPP2-(1-765 aa)-S479A also indicated that other unknown AMPK phosphosites on ASPP2 remained to be further investigated. We then investigated whether Ser479 phosphorylation was involved in apoptosis. HeLa cells were transfected with full-length ASPP2-WT or mutant ASPP2-S479A plasmids for 24 h. Apoptotic cells were labeled with Annexin V and PI dyes, and their fluorescence intensity was measured by flow cytometry. Compared to the control cells transfected with the vector only, overexpression of full-length ASPP2-WT significantly induced an increase in apoptosis (1.67 folds; $P < 0.05$, ANOVA); overexpression of mutant ASPP2-S479A appeared to increase the percentage of apoptotic cells, while the increase was not significant. Although there seemed a difference between the cells overexpressing full-length ASPP2-WT and those overexpressing mutant ASPP2-S479A, while the difference was not significant (Figure 3F). These results suggest that AMPK-mediated Ser479 phosphorylation partially contributed to ASPP2-induced apoptosis, but other AMPK phosphorylation sites on ASPP2 may also play roles in this process or there exist other unrecognized regulatory mechanisms.

Histone modification analysis characterized AMPK as a regulator of histone acetylation

Since chromatin-associated functions were highly enriched in bioinformatic analysis, we hypothesized that AMPK was involved in histone posttranslational modifications and epige-

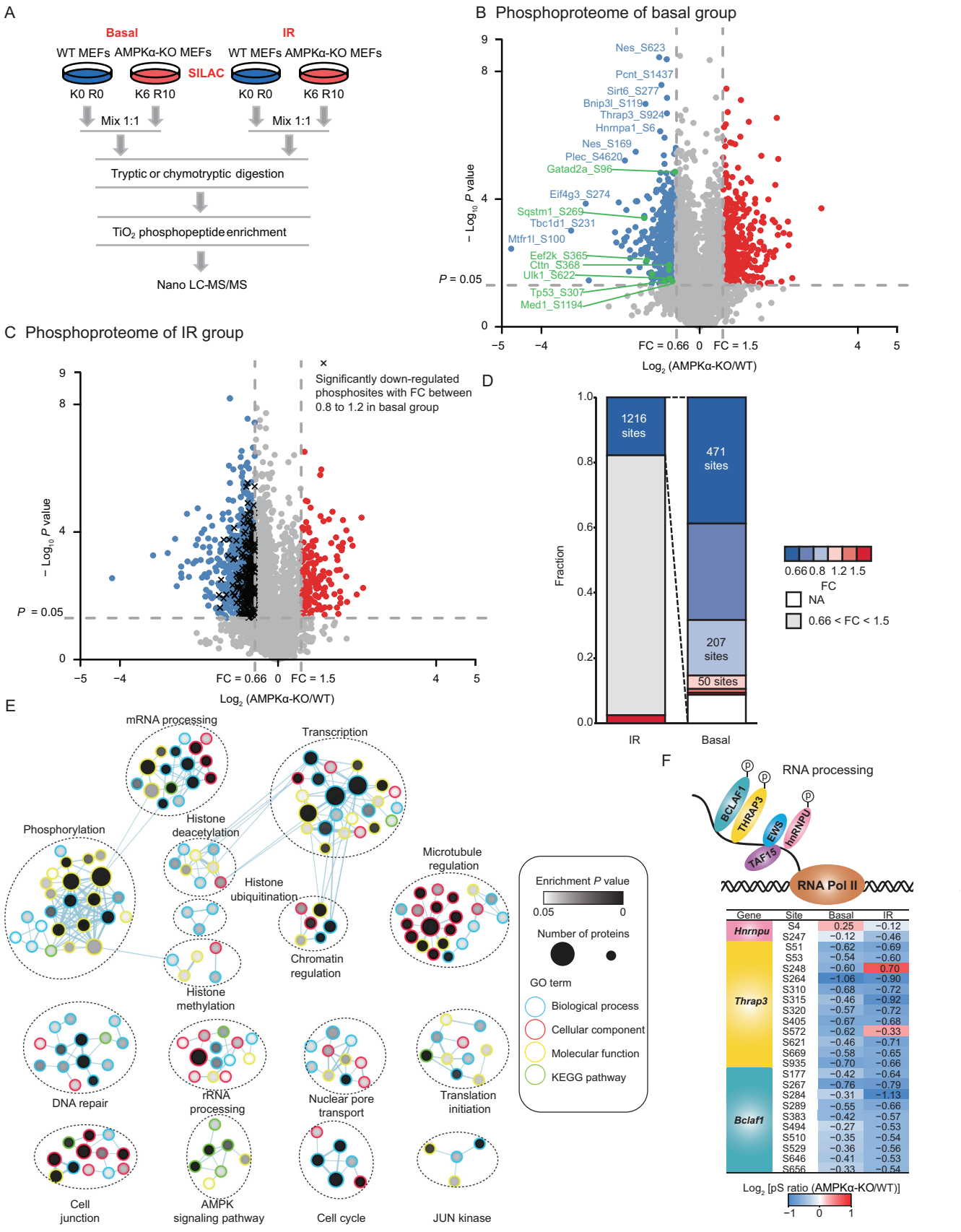
A
Basal
IR
WT MEFs AMPKα-KO MEFs
WT MEFs AMPKα-KO MEFs
SILAC
K0 R0
K6 R10
K0 R0
K6 R10
Mix 1:1
Mix 1:1
Tryptic or chymotryptic digestion
TiO2 phosphopeptide enrichment
Nano LC-MS/MS
B Phosphoproteome of basal group
Nes_S623
Pcnt_S1437
Sirt6_S277
Bnip3l_S119
Thrap3_S924
Hnrnpa1_S6
Nes_S169
Plec_S4620
Gatad2a_S96
Eif4g3_S274
Sqstm1_S269
Tbc1d1_S231
Mtfr1l_S100
Eef2k_S365
Cttn_S368
Ulk1_S622
Tp53_S307
Med1_S1194
P = 0.05
FC = 0.66
FC = 1.5
Log2 (AMPKα-KO/WT)
C Phosphoproteome of IR group
Significantly down-regulated phosphosites with FC between 0.8 to 1.2 in basal group
P = 0.05
FC = 0.66
FC = 1.5
Log2 (AMPKα-KO/WT)
D
1216 sites
471 sites
207 sites
50 sites
Fraction
IR
Basal
0.66 0.8 1.2 1.5
FC
NA
0.66 < FC < 1.5
E
mRNA processing
Transcription
Phosphorylation
Histone deacetylation
Histone ubiquitination
Microtubule regulation
Chromatin regulation
Histone methylation
DNA repair
rRNA processing
Nuclear pore transport
Translation initiation
Cell junction
AMPK signaling pathway
Cell cycle
JUN kinase
Enrichment P value
0.05
0
Number of proteins
GO term
Biological process
Cellular component
Molecular function
KEGG pathway
F
RNA processing
BCLAF1
THRAP3
EWS
hnRNPU
TAF15
RNA Pol II
Gene
Site
Basal
IR
Hnrnpu
S4 0.25 −0.12
S247 −0.12 −0.46
Thrap3
S51 −0.62 −0.69
S53 −0.54 −0.60
S248 −0.60 0.70
S264 −1.06 −0.90
S310 −0.68 −0.72
S315 −0.46 −0.92
S320 −0.57 −0.72
S405 −0.67 −0.68
S572 −0.62 −0.33
S621 −0.46 −0.71
S669 −0.58 −0.65
S935 −0.70 −0.66
Bclaf1
S177 −0.42 −0.64
S267 −0.76 −0.79
S284 −0.31 −1.13
S289 −0.55 −0.66
S383 −0.42 −0.57
S494 −0.27 −0.53
S510 −0.35 −0.54
S529 −0.36 −0.56
S646 −0.41 −0.53
S656 −0.33 −0.54
Log2 [pS ratio (AMPKα-KO/WT)]
−1 0 1

netic regulation. To address this question, we carried out a system-wide analysis to investigate the histone modification by MS in both non-IR basal status and IR stress status (**Figure 4**A). The heavy-labeled AMPKα-KO cells and light-labeled WT cells were mixed at a 1:1 ratio, and core histones (H2A, H2B, H3, and H4) were extracted and separated with SDS-PAGE. Histones were in-gel digested with trypsin into peptides and then subjected to MS analysis. The modified peptides were checked manually and quantified based on peak area integral according to the previous report [51]. Interestingly, AMPKα1/α2 KO resulted in significant up-regulation of global histone acetylation levels (Figure 4B; Table S2). Immunoblot assay also suggested increased acetylation levels at H2BK12, H3K18, and H4K16 in AMPKα1/α2-KO cell lines 1# and 2# (Figure 4C). These data suggest that AMPK plays a negative regulatory role in global histone acetylation.

To find out underlying regulation mechanism, we chose another potential substrate histone deacetylase 9 (HDAC9) from our phosphoproteome data for investigation. The amino acid sequence surrounding Ser239 of HDAC9 matched the AMPK substrate motif and was evolutionarily conserved (Figure 4D). Plasmids were synchronically introduced into 293T cells to overexpress Flag-HDAC9 and Myc-AMPKα2 for 48 h, and the whole cell lysates were subjected to exogenous IP assay using the anti-Flag antibody. AMPKα2 was detected using anti-Myc antibody in Flag-HDAC9 immunoprecipitated complex, suggested that AMPKα2 interacted with HDAC9 (Figure S5). Endogenous IP assay conducted in 293T cells further confirmed a reciprocal interaction between AMPKα2 and HDAC9 using anti-AMPKα2 and anti-HDAC9 antibodies (Figure 4E). Additionally, the exogenous fusion protein Flag-HDAC9 was enriched and extracted by anti-Flag antibody from 293T cells and incubated with activated or non-activated AMPKα2β2γ2 complex in kinase reaction buffer for 1 h. Phosphorylation signal (as measured by pan phospho-AMPK-substrate antibody) was detected on HDAC9 when incubated with activated-AMPKα2β2γ2 complex in the presence of CAMKKβ (Figure 4F). Taken together, HDAC9 was newly identified as a substrate of AMPK. Afterward, two plasmids expressing HDAC9-WT and phosphonull mutant HDAC9-S239A were constructed and introduced into 293T cells. Compared with negative control, overexpression of HDAC9-WT enhanced H2BK12 acetylation and H3K18 acetylation. In contrast, overexpression of phosphonull mutant HDAC9-S239A enhanced higher H2BK12 acetylation level but had no impact on H3K18 acetylation level (Figure 4G). Therefore, these results suggested that HDAC9 was involved in balance of histone acetylation while Ser239 phosphorylation on HDAC9 played a negative role in regulation of H2BK12 acetylation. Since there was no significant difference in HDAC9-Ser239 phosphorylation between basal and IR groups, AMPK likely phosphorylated HDAC9 at Ser239 in an IR-independent manner.

Taken together, quantitative phosphoproteome and histone modification analyses uncovered subtle crosstalk between AMPK-mediated phospho-regulation and histone acetylation.

JQ-1 synergizing with an AMPK inhibitor sensitizes cell apoptosis to IR

Histone acetylation had an impact on localized chromatin structures and played important roles in initiation and transduction of DNA damage signaling. BRD4, a member of the bromodomain and extraterminal (BET) family that binds acetylated histones H3 and H4, and regulates gene expression [52–54]. In addition to transcriptional regulation, BRD4 is essential in DDR and mediates the recruitment of chromatin-based repair proteins. Once sensing genome-wide DNA breaks, enhanced H4 acetylation led to BRD4 accumulation at breaks [51,55]. Since increased acetylation level at H3K14ac and global H4 acetylation level was observed in AMPKα-KO cells in basal group, but the tendency slightly attenuated after IR (Figure 4B), we hypothesized a potential linkage between AMPK and BRD4 during DDR. JQ-1, a BET inhibitor that impeded BRD4-acetylated lysine interaction, displayed anti-tumor activity in various types of cancer [56,57]. Interestingly, JQ-1 treatment made AMPKα-KO cells more sensitive to IR than WT cells (**Figure 5**A). Similarly, we found JQ-1 treatment together with Compound C (an AMPK inhibitor) improved the sensitivity of M059J glioma cells to IR, especially in a relatively high dose (Figure 5B). It was suggested that acetylation of histones H3K14, H4K12, and H4K16 were important for BRD4 binding [58]. In consistency, JQ-1 reduced acetylation of H3K14 and H3K18 in both WT and AMPKα-KO cells. However, quite different effects of JQ-1 on the acetylation of H3K23 and H2BK12 were observed in WT and AMPKα-KO cells. JQ-1 treatment had no effect on H3K23 acetylation in WT cells but reduced H3K23 acetylation

Figure 2 Quantitative phosphoproteomics uncovered broad signaling pathways regulated by AMPK in DDR
A. General workflow of quantitative phosphoproteomic analysis. The SILAC-labeled WT and AMPKα-KO MEF cells in basal or IR group were lysed and mixed together. Phosphopeptides were enriched and analyzed by Nano LC-MS/MS. Two replicates were analyzed. **B.** Volcano plot of quantitative phosphoproteomics analysis of basal group. The phospho-peptides with FC (AMPKα-KO/WT) > 1.5 (P value < 0.05) were selected as significantly regulated. Red dots were the phosphosites significantly up-regulated. Blue dots were the phosphosites significantly down-regulated. Green dots were the phosphosites on known AMPK substrates. **C.** Volcano plot of quantitative phosphoproteomics analysis of IR group. Cross represented the phosphosites which were significantly down-regulated in IR group (FC < 0.66) but are unchanged in basal group (0.8 < FC < 1.2). **D.** The bar graph showing the changes of up-regulated phosphosites after IR in basal group. **E.** Representative enrichment results from phosphoproteomics analysis. Proteins with significantly down-regulated phosphorylation after IR were analyzed for GO term and KEGG pathway enrichment using DAVID. Visualization of results was performed with Cytoscape and EnrichmentMapApp. Nodes represent a gene set with enriched GO terms or KEGG pathways. Edges represent sharing proteins among nodes. Terms visualized have a P value cutoff of < 0.05. **F.** The diagram showing the significantly changed phosphosites in RNA processing. FC, fold change.

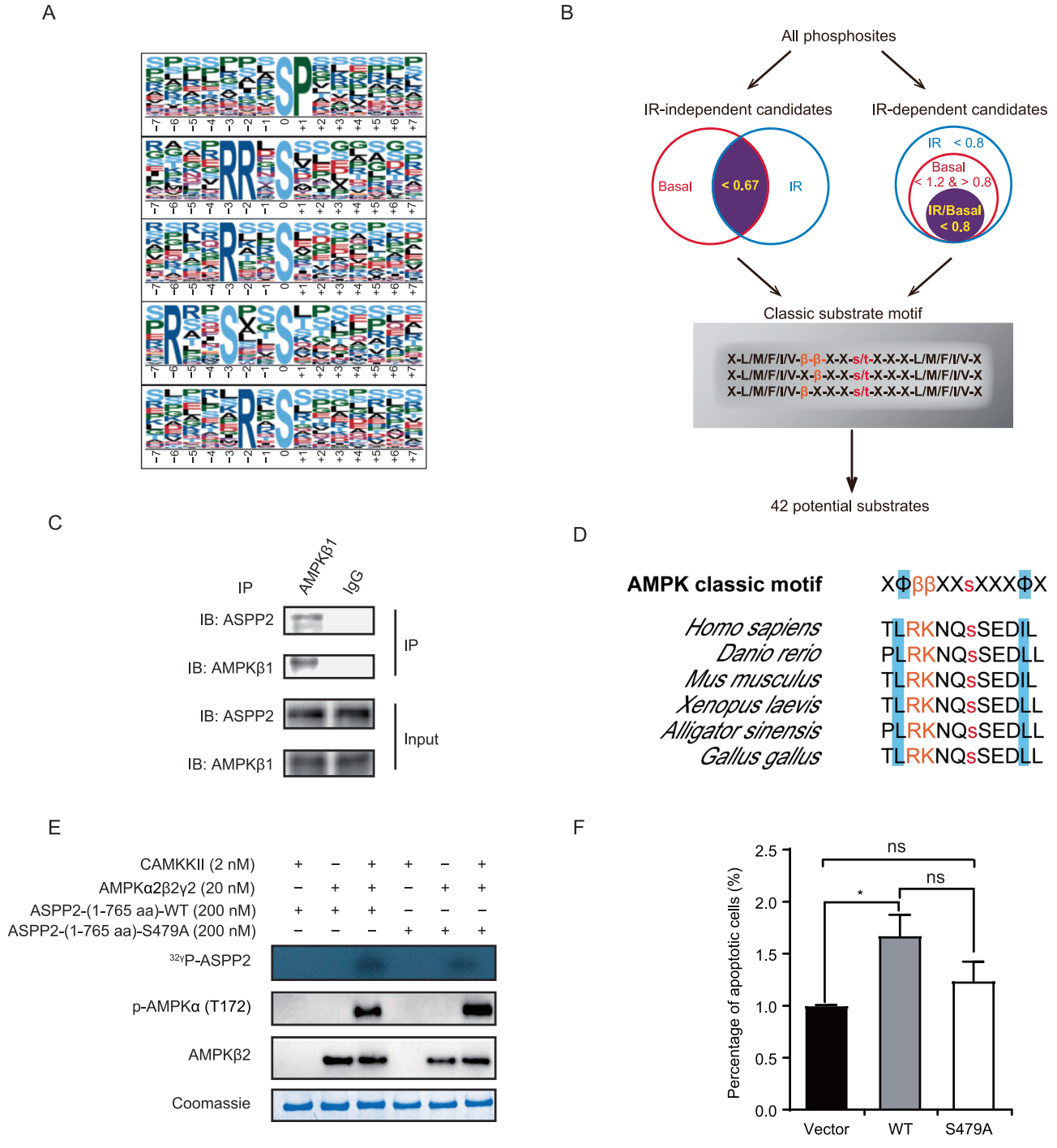

Figure 3 Bioinformatic analysis identified ASPP2 as a novel substrate of AMPK involved in apoptosis

A. Motif analysis of significantly down-regulated phosphosites in IR group by Motif-X. **B.** Strategy diagram for identification of candidate AMPK substrates. **C.** ASPP2 interacts with AMPKβ1 *in vivo*. Endogenous Co-IP was performed in 293T cells using anti-AMPKβ1 antibody. **D.** The evolutionarily conserved amino acid sequence surrounding Ser479 on ASPP2 matches the consensus AMPK phosphorylation motif. **E.** AMPK phosphorylates ASPP2 at Ser479 *in vitro*. *In vitro* kinase assays were performed using 200 nM truncated ASPP2-(1-765 aa)-WT/S479A, 20 nM AMPKα2β2γ2 (inactive or active), 0.1 mM DTT, and 5 μCi γ-[^{32}P] ATP per reaction. **F.** AMPK-mediated Ser479 phosphorylation partially contributed to ASPP2-induced apoptosis. HeLa cells with ectopic overexpression of full-length ASPP2-WT or phosphonull ASPP2-S479A mutant were stained by PI and FITC-AnnexinV dyes, and the fluorescence intensity was recorded by flow cytometer. Data are analyzed with one-way ANOVA followed by Fisher's LSD tests with two-tailed distribution using GraphPad Prism software. Data are presented as mean ± SEM. *, $P < 0.05$; ns, not significant. IP, immunoprecipitation; Co-IP, co-immunoprecipitation.

Table 1 The candidate AMPK substrates identified by quantitative phosphoproteomics

Type	Gene name	Site	Sequence window	Basal log_2 ratio	IR log_2 ratio
IR-dependent substrate candidate	*Ampd2*	S_135	FLKTDSDSDLQ	–0.08	–0.85
	Atp2b1	S_252	FRIEDSEPHIP	–0.19	–1.05
	Atp6v0a2	S_695	LVRKDSEEEVS	0.16	–0.46
	Ccnyl1	S_276	MRRSLSADNFI	–0.11	–1.23
	Cdc42ep1	S_121	IKNAISLPQLN	–0.21	–0.51
	Cdc42ep1	S_207	LRRSDSLLSFR	–0.21	–0.64
	Cdk17	S_137	IHRRISMEDLN	0.09	–0.55
	Clasp2	S_376	LQRSRSDIDVN	–0.09	–0.77
	Mtmr3	S_613	LPKTRSFDNLT	–0.02	–0.47
	Net1	S_508	FQRAASPLELQ	0.19	–0.41
	Plekhg5	S_906	LLKSKSEASLL	0.08	–0.37
	Ppfibp1	S_435	LQKSSSLGNLK	0.13	–0.33
	Ppp1r12c	S_375	LQRSASSSLLE	0.02	–0.58
	Prpsap2	S_227	VDGRHSPPMVR	–0.17	–0.66
	Scrib	S_1206	LGHRNSLESIS	–0.01	–0.45
	Skiv2l	S_253	LVRASSLEDLV	0.00	–0.52
	Syne2	S_4097	LSRTNSMSFLP	–0.23	–0.78
	Tbc1d25	S_378	LLRQASLDGLQ	–0.04	–0.38
	Tnks1bp1	S_866	FGKRDSLGSFS	–0.20	–0.45
	Tp53bp2	S_479	LRKNQSSEDIL	–0.07	–0.49
	Zdhhc8	S_603	VLRYGSRDDLV	–0.08	–0.78
IR-independent substrate candidate	*Arhgef1*	S_831	LKPRPSPSSIR	–0.71	–1.25
	Cdr2l	S_179	FRLHSSSLELG	–0.94	–1.25
	Cobll1	S_1011	LRAETSPPPVF	–0.69	–0.61
	Dennd4a	S_1241	LTNKKSPTLVK	–0.98	–1.13
	Epb41l2	S_86	LKKQRSYNLVV	–0.56	–0.90
	Gpatch8	S_1039	IYRSQSPHYFQ	–0.84	–0.70
	Hdac9	S_237	VAERRSSPLLR	–2.62	–1.46
	Klc3	S_467	MKRAMSLNMLN	–0.67	–0.97
	Larp4b	S_603	FERSPSPVHLP	–0.58	–0.76
	Lnp	S_411	VLRADSVPNLE	–0.82	–0.83
	Mis18bp1	S_215	LHSKESPVRIT	–0.78	–0.88
	Mtfr1l	S_100	MQRNASVPNLR	–4.77	–4.20
	Nek1	S_972	MLRTCSLPDLS	–0.97	–1.00
	Ppp1r13l	S_102	FGRSESAPSLH	–0.79	–0.83
	Ralbp1	S_29	LTRTPSSEEIS	–0.78	–0.83
	Ralgapa1	S_796	LPRSSSTSDIL	–1.07	–0.60
	Sphk2	S_364	LPRAKSELVLA	–1.24	–1.80
	Srrm2	S_2084	LDRCRSPGMLE	–0.59	–0.85
	Srrm2	S_2535	LKRVPSPTPVP	–0.60	–0.72
	Taok1	S_965	MGVRNSPQALR	–0.70	–0.79
	Zfc3h1	S_356	LTRRLSASDIV	–0.86	–0.84

in AMPKα-KO cells. In contrast, JQ-1 treatment did not change H2BK12 acetylation in AMPKα-KO cells but reduced H2BK12 acetylation in WT cells (Figure 5C and D). Notably, JQ-1 reduced histone acetylation before IR, with no obvious changes observed after IR, suggesting that JQ-1 regulated histone acetylation in an IR-independent manner. Since WT and AMPKα-KO cells showed an opposite trend on H2BK12 and H3K23 acetylation after JQ-1 treatment, we hypothesized that AMPK signaling and BRD4 signaling coordinately regulated H3K23 and H2BK12 acetylation. Next, we investigated how the JQ-1-induced basal changes in histone acetylation finally resulted in lower cell viability under IR stress. Herein, we investigated whether repair signaling activated normally by JQ-1 treatment resulted in enhanced phospho-KAP-1(Ser824) signals and prolonged γH2A.X signals sustained in AMPKα-KO cells, but without changes in phospho-p53 (Ser15) (Figure 5E). Therefore, we hypothesized that JQ-1 treatment affected the chromatin relaxation by disrupting the orchestrated regulation of histone acetylation during DDR. Accumulated unrepaired DSB ends, as indicated by enhanced γH2A.X signals, would induce apoptosis. Consistently, we observed that JQ-1 treatment induced a higher proportion of apoptotic cells in the AMPKα-KO cells than in WT cells (Figure 5F). Thus, we concluded that AMPKα1/α2 KO disrupted the orchestrated histone acetylation, which promoted the pro-apoptotic effect induced by JQ-1 treatment during DDR. Taken together, inhibition of AMPK activity improved the anti-tumor efficacy of JQ-1 via disrupting the balance in histone acetylation.

Discussion

AMPK is an essential eukaryotic energy sensor to coordinate metabolism and other biological activities. LKB1, one of the upstream kinases of AMPK, was a well-defined tumor suppressor [59]. However, fully understanding the exact role of AMPK seemed challenging. Previous studies suggested that AMPK, unlike its upstream kinase, played contradictory roles in tumor progression and therapy. AMPK activation regulated

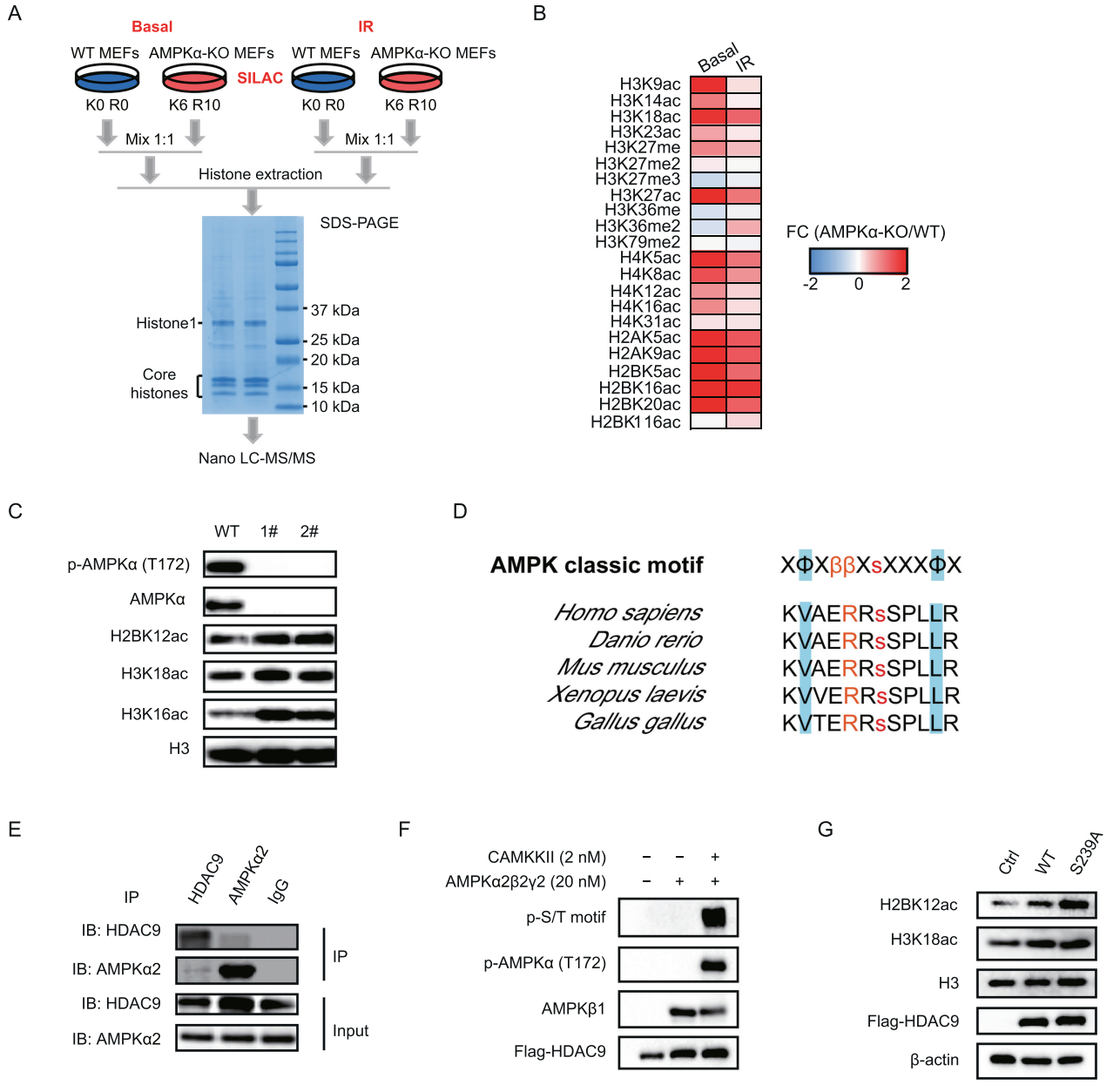

Figure 4 Histone modification analysis characterized AMPK as a regulator of histone acetylation

A. General workflow for quantification of histone modification. The SILAC-labeled WT and AMPKα-KO MEF cells in basal or IR group were lysed and mixed together. Histones were extracted and analyzed by Nano LC-MS/MS. **B.** The quantified histone marks in response to DNA damage in AMPKα-KO MEF cells. The FC of histone posttranslational modifications in AMPKα-KO MEF cells compared to WT MEF cells in basal or IR group was detected by LC-MS/MS. **C.** AMPKα1/α2 KO changes global histone acetylation. Both WT and AMPKα1/α2 KO cells (1# and 2#) were subjected to immunoblot for validation of results presented in (B). **D.** The evolutionarily conserved amino acid sequence surrounding Ser239 on HDAC9 matches the consensus AMPK phosphorylation motif. **E.** HDAC9 interacts with AMPKα2 *in vivo*. Endogenous Co-IP was performed in 293T cells using anti-AMPKα2 and anti-HDAC9 antibodies. **F.** AMPK phosphorylates HDAC9 at Ser239 *in vitro*. *In vitro* kinase assays were performed using immunoprecipitated Flag-HDAC9, 20 nM AMPKα2β2γ2 (inactive or active), 0.1 mM DTT, and 0.1 mM ATP per reaction. The reaction sample was subjected to immunoblot using the pan phospho-AMPK substrate antibody. **G.** Phosphonull HDAC9-Ser239A mutant affected the H2BK12 acetylation. 293T cells were transfected with plasmids to overexpress HDAC9-WT and HDAC9-Ser239A mutant for 48 h and then subjected to immunoblot.

diverse downstream signaling pathways, together with complicated tumor microenvironments, which led to context-dependent cell fates. In one hand, AMPK phosphorylated ULK1 and promoted cell autophagy, to maintain cell survival in conditions of hypoxia and low nutrition [16,60]. On the other hand, AMPK negatively regulated TSC-mTOR axis and inhibited cell outgrowth under the circumstance of energy deprivation [61–63]. It seemed that cell fate resulted from

AMPK activation mainly depended on comprehensive signaling network within heterogenic tumor cells. The intercellular signaling network in types of tumors was balanced and maintained by both extrinsic stimulators like hypoxia and growth factors, as well as intrinsic features like gene signatures and transcriptional regulation [64,65]. Genome instability and mutation was defined as one of the hallmarks in various types of cancer [66]. Abnormal DNA repair, especially dysfunctional DSB repair, has an impact on the genetic fidelity and chromatin structure and consequently leads to genome instability and mutation [32,67]. Previous studies suggested that AMPK was involved in DNA-damaging agent induced cell apoptosis, but the underlying mechanism remained to be further understood [34,68,69]. Meanwhile, several studies shed light on the linkage between AMPK and DDR. DDR is a critical process to activate accurate repair pathways and other biological processes to coordinately repair damages. Therefore, a comprehensive understanding of the AMPK's role in DDR is a critical step toward understanding the exact role of AMPK in tumor biology.

To address the question, we designed a study to investigate whether novel AMPK substrates were involved in DDR. We carried out a system-wide phosphoproteomic study and global histone posttranscriptional modification analysis. Bioinformatic analysis of significantly altered phosphoproteins enriched DNA damage repair-associated events and chromatin-associated functions, suggesting complicated regulatory network of AMPK in DDR. After comparing these altered phosphosites to classic AMPK substrates, we totally obtained 42 potential substrates of AMPK from basal group and IR group. This result suggested that although IR might dramatically induce phosphorylation changes, AMPK likely had limited direct impact on DNA-associated signaling pathways.

Corresponding to the fact that chromatin-associated functions were enriched in phosphoproteomic study, histone modification analysis also suggested that AMPK negatively regulated global histone acetylation. Therefore, an integrative analysis of two studies implicated a crosstalk between AMPK-mediated phospho-regulation and histone acetylation. Based on this result, we further identified HDAC9, a member of Class IIa histone deacetylase family, as a new substrate phosphorylated by AMPK in an IR-independent manner. Overexpression of WT HDAC9 in cells increased the acetylation level at H2BK12 and H3K18, and the non-phosphorylatable mutant HDAC9-S239A further promoted the increase of H2BK12 acetylation. Thus, we concluded that AMPK-mediated phosphorylation on HDAC9 might be required in balancing the histone acetylation at H2BK12, but the mechanism remained to be further investigated.

It was worth noting that AMPK-mediated phosphorylation at Ser479 of ASPP2 partially contributed to ASPP2-induced apoptosis in an IR-dependent manner. p53 plays distinct roles via different co-factors in DDR, including induction of cell cycle arrest or apoptosis. ASPP2 is the co-factor of p53 required in spontaneous induction of apoptosis and cooperates with p53 to suppress tumor growth [70,71]. Previous studies suggested that a high level of ASPP2 sensitized cells to IR and DNA-damaging agents [72,73]. Overexpression of non-phosphorylatable mutant ASPP2-S479A moderately impaired apoptosis, suggesting that AMPK promoted apoptosis during DDR by phosphorylating ASPP2 at Ser479. The accumulation of unrepaired DNA damages activated apoptosis signaling pathway, thus avoiding hereditary of abnormal genetic information in mitosis. Taken together, AMPK-ASPP2 axis promoted apoptosis to prevent cells from genomic instability caused by sustained damages during DDR. Further study might focus on whether the phosphorylation site influenced protein interaction of ASPP2 complex and its correlation with cancer incidence or drug resistance.

Finally, our findings might reveal a crosstalk between AMPK activity and histone acetylation in tumor biology. Indeed, disturbing the histone acetylation by BRD4 inhibitor JQ-1 enhanced the sensitivity of cells to IR via induction of apoptosis. It was worth noting that except for H3K14ac, JQ-1 also influenced acetylation at H2BK12, H3K23, and H3K18. Additionally, AMPKα1/α2-deficient cells were more sensitive than WT cells to JQ-1 treatment. These results suggested the potential role of AMPK in cancer therapy. First, AMPK activity might be used as a biomarker to predict the therapeutic response to acetyltransferase inhibitors or deacetylase inhibitors. Second, selective AMPK inhibitor might be useful to improve the sensitivity of tumor cells to radiotherapy or target-therapy.

Therefore, our study provided a source of AMPK-associated phosphorylation network and histone acetylation events, which might be helpful to understand the role of AMPK in DDR.

Materials and methods

Antibodies and compounds

The primary antibodies Phospho-Histone H2A.X (Ser139) (Catalog No. 2577), Phospho-p53 (Ser15) (Catalog No. 9284), Phospho-AMPKα (Thr172) (Catalog No. 2535), Phospho-Acetyl-CoA Carboxylase (Ser79) (Catalog No. 3661), Acetyl-CoA Carboxylase (Catalog No. 3662), AMPKα (Catalog No. 2532), AMPKα2 (Catalog No. 2757), AMPKβ1 (Catalog No. 12063), AMPKβ2 (Catalog No. 4148), GAPDH (Catalog No. 2118), and Myc-Tag (9B11) (Catalog No. 2276) were bought from Cell Signaling Technology (Danvers, MA). The primary antibodies Phospho-KAP1 (Ser824) (Catalog No. ab70369), H2B-Acetyl-K12 (Catalog No. ab61228), H4-Acetyl-K16 (Catalog No. ab109463), H3-Acetyl-K14 (Catalog No. ab82501), H3-Acetyl-K18 (Catalog No. ab1191), H3-Acetyl-K23 (Catalog No. ab61234), and 53BP2 (Catalog No. ab236448) were bought from Abcam (Cambridge, UK). The primary antibody HDAC9 (Catalog No. MA5-32820) was bought from ThermoFisher Scientific (Waltham, MA). The DYKDDDDK Tag (Catalog No. 018-22783) was bought from Wako (Osaka, Japan). The antibody β-actin (Catalog No. AM1021B) was bought from Abgent (San Diego, CA).

Secondary antibody Alexa Fluor 555 labeled donkey anti-rabbit IgG (Catalog No. A31572) and Hoechst 33342 Solution (Catalog No. 62249) were bought from ThermoFisher Scientific. The secondary peroxidase AffiniPure Goat Anti-Mouse IgG (H + L) (Catalog No. 115-035-003) and Peroxidase AffiniPure Rabbit Anti-Goat IgG (H + L) (Catalog No. 305-035-003) were bought from Jackson ImmunoResearch Laboratories (West Grove, PA). Chemiluminescent detection was completed with enhanced chemiluminescence (ECL) Western blotting reagents (Catalog No. RPN2236, GE Healthcare, Chicago, IL).

The compound JQ-1 (Catalog No. S7110) was bought from Selleck (Houston, TX). The AMPK activator AICAR (Catalog No. A9978) and AMPK inhibitor (Catalog No. 171260) were bought from Sigma (St. Louis, MO) and Millipore (Burlington, MA), respectively.

Cell culture and stable isotope labeling by amino acids in cell culture labeling

WT MEFs and AMPKα1/α2-KO MEF cell lines were cultured in DMEM with light lysine ($^{12}C_6^{14}N_2$-Lys) and arginine ($^{12}C_6^{14}N_4$-Arg), or heavy lysine ($^{13}C_6^{14}N_2$-Lys) and arginine ($^{13}C_6^{15}N_4$-Arg), respectively. The proteome labeling efficiency of heavy isotopic amino acids was >98%, as determined by MS analysis. The HeLa and 293T cells were cultured in DMEM growth medium (Catalog No. 12100061, Gibco, Carlsbad, CA) supplemented with 10% FBS (Catalog No. 10099, Gibco). The M059J cells were grown in a medium containing a 1:1 mixture of DMEM and F12 medium (Catalog No. 11330057, Gibco) supplemented with 10% FBS. All cells were cultured at 37 °C with 5% CO_2.

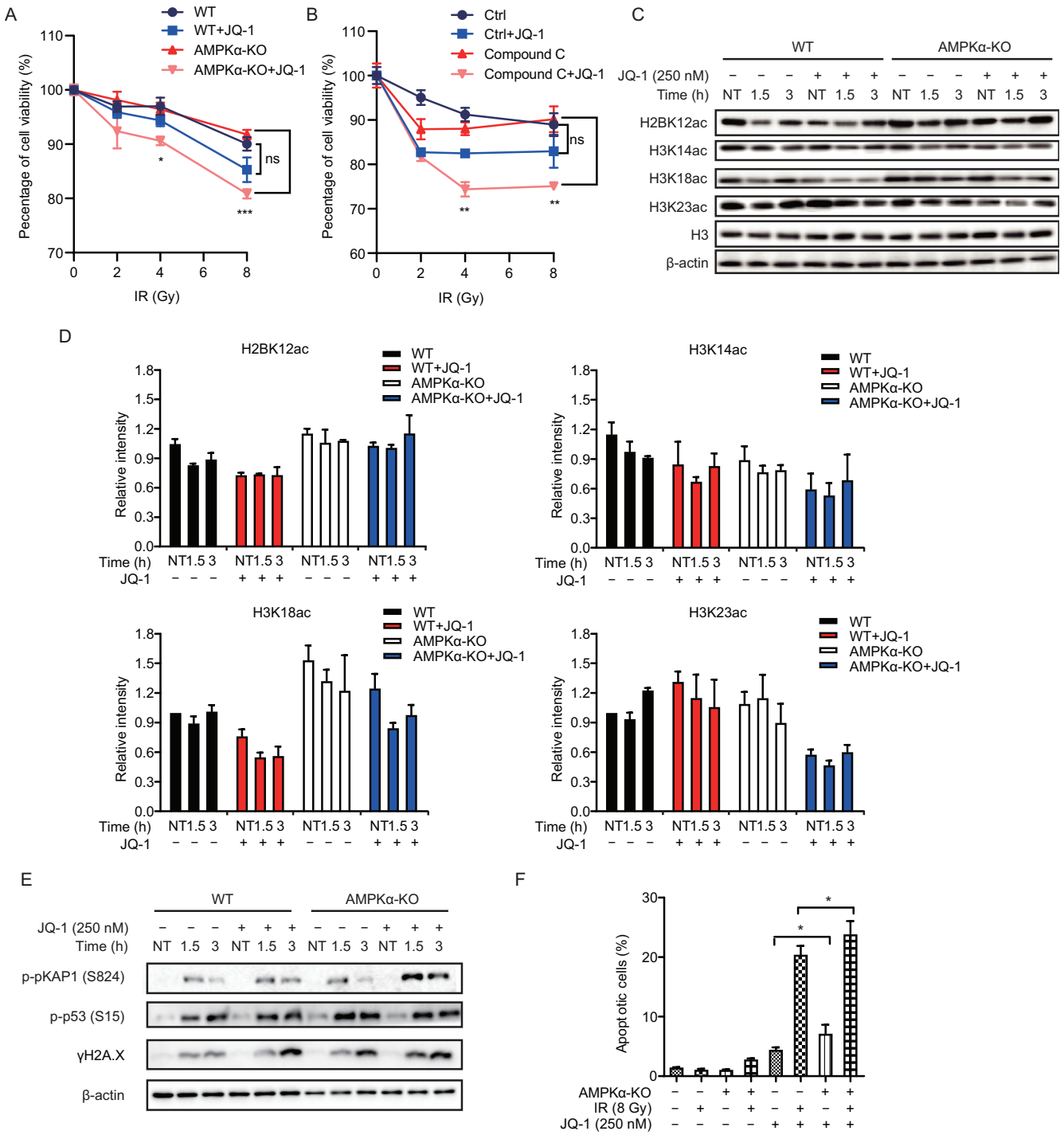

Protein lysate preparation and in-solution digestion

Cells were harvested and washed with pre-cold phosphate-buffered saline (PBS). Then, cells were lysed with lysis buffer (8 M Urea in 100 mM NH_4HCO_3) and subjected to sonication. After sonication, the lysates were clarified by centrifugation at 21,130 *g* for 10 min. Equal amounts of WT and AMPKα1/α2-KO MEF cell lysate were mixed. The cell lysate mixture was reduced by 5 mM dithiothreitol (Catalog No. D0632, Sigma) at 56 °C for 30 min. Then 15 mM iodoacetamide (Catalog No. I6125, Sigma) was added to alkylate the sulfhydryl groups. The extra iodoacetamide was eliminated using 30 mM cysteine. The protein extract was digested with trypsin (Catalog No. V5280, Promega, Madison, WI) (trypsin:protein = 1:50) at 37 °C for 12 h. For complete digesting, additional trypsin (trypsin:protein = 1:100) was added for another 4 h. Same amount of protein extract was digested with chymotrypsin (Catalog No. 11418467001, Roche, Basel, CHE) (chymotrypsin:protein = 1:50) at 25 °C for 18 h. Both tryptic and chymotryptic peptides were desalted through Waters Sep-Pak C18 cartridges (Catalog No. WAT054960, Waters, Milford, MA), vacuum-dried, and stored at −80 °C for further analysis.

Histone extraction and in-gel digestion

Histone extraction was carried out as previously published [74,75]. The isolated cells were lysed with extraction buffer (10 mM HEPES, 10 mM KCl, 1.5 mM $MgCl_2$, 0.5% NP-40, 1× protease inhibitor mixture). Lysate was centrifuged at 1000 *g* at 4 °C. Then, the pellets were washed and resuspended in 0.2 M H_2SO_4 overnight at 4 °C. The mixture was clarified by centrifugation, and the supernatant was collected for trichloroacetic acid precipitation. The precipitate was washed with pre-cold acetone several times. The precipitate was dried completely at room temperature and then dissolved in water for SDS-PAGE separation. Bands of histones (H1, H2A, H2B, H3, and H4) were excised and subjected to in-gel digestion. The tryptic peptides were analyzed by LC-MS/MS. After MS analysis, histone modifications of H2A, H2B, H3, and H4 were quantified by examined the peak area of modified peptide ions.

Phosphopeptide enrichment

Phosphopeptide enrichment was carried out as previously published [51]. In brief, tryptic peptides were dissolved in loading buffer (6% TFA, 80% ACN, 1 M lactic acid), and then incubated with titanium dioxide beads (GL Sciences, Japan) at room temperature at a proportion of peptide: TiO_2 = 4:1. The titanium dioxide beads were then washed with loading buffer for three times, wash buffer A (0.5% TFA, 30% ACN) for one time and wash buffer B (0.5% TFA, 80% ACN) for two times. The phosphopeptides were eluted from the beads with 15% NH_3H_2O and separated into six fractions.

Nano-HPLC-MS/MS analysis

The peptides were analyzed by an EASY-nLC 1000 system (ThermoFisher Scientific) connected to an Orbitrap Q-Exactive mass spectrometer (ThermoFisher Scientific). Peptides were eluted from a reverse-phase C18 column (75 μm ID, 3 μm particle size, Dikma Technologies Inc., CA) with a 70 min gradient of 7%-to-80% buffer B (90% acetonitrile, 10% H_2O, 0.1% formic acid) at a flow rate of 300 nl/min. Full MS spectra with an m/z range of 350–1300 were acquired with a resolution of 70,000 at m/z = 200 in profile mode. The AGC targets were 1.0e6 for full scan and 1.0e6 for MS/MS scan, respectively. Fragmentation of the 16 most intense precursor ions occurred at the HCD collision cell with a normalized collision energy of 28%, and tandem MS were obtained with a resolution of 17,500 at m/z = 200. Dynamic exclusion duration was set as 60 s.

MS data analysis

MS/MS data were processed using MaxQuant software (version 1.5.3.2). *Mus musculus* database from UniProt (release 2018_10_13, 53,781 entries) with a reversed decoy database

Figure 5 JQ-1 synergizing with an AMPK inhibitor induces cell apoptosis to IR

A. JQ-1 treatment sensitizes AMPKα1/α2-KO cells to IR. Both WT and AMPKα-KO cells were pretreated with 250 nM JQ-1 for 12 h and then exposed to increasing doses of X-ray (0, 2, 4, and 8 Gy). After 72 h, the cell viability was detected by MTS assay. Each group was normalized to NT (0 Gy), respectively. Data are analyzed with one-way ANOVA followed by Fisher's LSD tests with two-tailed distribution using GraphPad Prism software. Data are presented as mean ± SEM. *, $P < 0.05$; ***, $P < 0.001$; ns, not significant. **B.** JQ-1 synergizing with an AMPK inhibitor sensitizes cells to IR. M059J cells were pretreated with 250 nM JQ-1 for 12 h, and then 1 μM Compound C (an AMPK inhibitor) was added to the culture medium 2 h before IR. Then the cells were exposed to increasing doses of X-ray (0, 2, 4, and 8 Gy) and allowed for recovery for 72 h before cell viability assay was performed by MTS assay. Each group was normalized to NT (0 Gy), respectively. Data are analyzed with one-way ANOVA followed by Fisher's LSD tests with two-tailed distribution using GraphPad Prism software. Data are presented as mean ± SEM. **, $P < 0.01$; ns, not significant. **C.** AMPKα1/α2 KO disrupts the response of histone acetylation to JQ-1 treatment. Both WT and AMPKα-KO cells were pretreated with 250 nM JQ-1 for 12 h and then exposed to a single dose of 10 Gy X-ray. The cells were harvested at the indicated time points and analyzed by immunoblot. **D.** Quantitative result of (C) is measured by ImageJ software. Data are shown as mean ± SEM from two independent experiments. **E.** AMPKα1/α2 KO prolongs heterochromatin relaxation signals caused by JQ-1 treatment. The samples were collected simultaneously as in (C) and analyzed by immunoblot. **F.** JQ-1 treatment sensitizes AMPKα1/α2-KO cells to IR. WT and AMPKα-KO cells were pretreated with 250 nM JQ-1 for 12 h and then exposed to a single dose of 10 Gy X-ray. 24 h post IR, cells were harvested and stained by PI/FITC-AnnexinV dyes, and the fluorescence intensity was recorded by FACS. Data are normalized to the negative control (WT without IR and JQ-1 treatment). Data are analyzed with one-way ANOVA followed by Fisher's LSD tests with two-tailed distribution using GraphPad Prism software. Data are shown as mean ± SEM from two independent experiments. *, $P < 0.05$.

was used for data processing. For database searching, trypsin was set as the specific enzyme and the maximum number of missed cleavages was fixed at 2. Carbamidomethylation of cysteine residues was set as a fixed modification; oxidation of methionine and protein N-terminal acetylation were set as variable modifications. Phosphorylation of serine, threonine, and tyrosine was set as variable modification for phosphosite analysis. Precursor mass tolerance for MaxQuant analysis was set to 4.5 ppm and MS/MS tolerance was set to 20 ppm. FDR thresholds for protein, peptide, and modification sites were all set as 1%.

Bioinformatic analysis

DAVID bioinformatics functional annotation tool was used to identify enriched GO and KEGG pathway terms. *Mus musculus* genome was used as background in DAVID functional annotation analysis. The significance of fold enrichment was calculated using $P < 0.05$. Gene sets with $P < 0.05$ were visualized in enrichment maps using EnrichmentMapApp and Cytoscape. Motif-X was used to identify phosphorylation motifs present in significantly changed phosphoproteins.

In vitro kinase assay and autoradiography

Briefly, the recombinant AMPKα2β2γ2 complex (200 nM) was pre-incubated with 20 nM CAMKKβ to be fully activated in reaction buffer (5 mM $MgCl_2$, 20 mM Tris-HCl, 8 nM ATP, 1 mM DTT) at 37 °C for 1 h. Then 200 nM substrate was incubated with 20 nM activated AMPK in reaction buffer at 37 °C for 1 h, in which ATP was replaced by [^{32}P]-labeled ATP (Catalog No. BLU002250UC, Perkin Elmer, Waltham, MA). Afterward, the reaction mixture was terminated by SDS loading buffer and subjected to immunoblot analysis. Then SDS-PAGE was sealed with photographic film together for 12 h before the film was fixed.

Co-immunoprecipitation

Interested plasmids were introduced into 293T cells for 48 h, then 293T cells overexpressing targeted proteins were lysed by buffer A (Catalog No. P0013B, Beyotime Biotechnology, Shanghai, China) (supplemented with 10 mM NaF, 1 mM Na_2VO_3, and protease inhibitor cocktails). The lysates were centrifuged at 10,000 r/min, 4 °C for 10 min. The separated supernatant was divided into three fractions and respectively incubated with negative IgG or reciprocal antibodies at 4 °C overnight. Then pre-processed protein A agarose (Catalog No. P3476, Sigma) was added to mixture. After another 2-h incubation, the bead-antibody-protein complex was isolated from mixture by centrifuging at 1000 r/min, 4 ℃ for 5 min. To remove the non-specific binding proteins, the bead-antibody-protein complex was washed with pre-cold PBS buffer for three times before the samples were subjected to immunoblot assay.

Cell viability assay

Both WT and AMPKα-KO MEF cells (5000 per well) were pre-treated with 250 nM JQ-1 for 12 h, followed by exposure to increasing doses of X-ray (0, 2, 4, and 8 Gy).

M059J cells (7500 per well) were pre-treated with 250 nM JQ-1 and 1 μM Compound C for 12 h, followed by exposure to increasing doses of X-ray (0, 2, 4, and 8 Gy). After 72-h recovery, the cells were subjected to MTS assay according to the manufacturer's instructions. 10 μl per well of MTS/PMS (20:1, Promega) solution was added to each well containing 100 μl of culture medium, followed by a gentle shake. After incubation at 37 °C under 5% CO_2 for 4 h, the absorbance of the solutions was measured at 490 nm, using an M5 microplate reader (Molecular Device, San Jose, CA).

Cell cycle assay

Both WT and AMPKα-KO MEF cells (7.5×10^4/well) were exposed to a single dose of 8 Gy X-ray. After 24-h recovery, cells were sampled by EDTA-free trypsin and 75% ethanol. Fixed cells were then incubated with 50 μg/ml propidium iodide (Catalog No. P4170, Sigma) and 100 μg/ml RNaseA (Catalog No. ST576, Beyotime Biotechnology) for 15 min at room temperature. The mean fluorescence intensity of DNA content was recorded by Flow cytometer (NovoCyte D2060R, San Diego, CA) by PE channel. 10,000 events per sample were collected and analyzed by Software NoveExpress.

Cell apoptosis assay

The cell apoptosis assay was performed by Annexin V-FITC/PI apoptosis detection kit (Catalog No. KGA108, KeyGEN BioTECH, Nanjing, China) according to the manufacturer's instructions. Briefly, 2×10^5 cells were prepared according to experimental design. At the sample point, cells were digested with EDTA-free trypsin and incubated with staining solution (500 μl Detection Buffer supplemented with 5 μl PI and 5 μl Annexin-V) for 15 min at room temperature. The fluorescence intensity was recorded by Flow cytometer (NovoCyte D2060R) by FITC and PE channel after fluorescence compensation deduction. 15,000 events per sample were collected and analyzed. Total apoptotic cells were $FITC^+PI^-$ cells plus $FITC^-PI^+$ cells. Data are presented as a densitometric ratio change normalized to the negative control.

Data availability

All MS raw data have been deposited to the ProteomeXchange Consortium via the iProX partner repository (ProteomeXchange: PXD039113; iProX: IPX0001446000), which are publicly accessible at http://proteomecentral.proteomexchange.org and https://www.iprox.cn, respectively.

CRediT author statement

Yuejing Jiang: Conceptualization, Methodology, Validation, Formal analysis, Investigation, Data curation, Writing - original draft, Writing - review & editing, Visualization. **Xiaoji Cong:** Methodology, Software, Data curation, Formal analysis, Investigation, Data curation, Writing - original draft, Writing - review & editing, Visualization. **Shangwen Jiang:** Methodology, Software, Formal analysis, Investigation. **Ying Dong:** Formal analysis, Investigation. **Lei Zhao:** Software, Investigation. **Yi Zang:** Conceptualization, Resources, Writing

- original draft, Writing - review & editing, Supervision, Project administration, Funding acquisition. **Minjia Tan:** Conceptualization, Resources, Writing - original draft, Writing - review & editing, Supervision, Project administration, Funding acquisition. **Jia Li:** Conceptualization, Resources, Supervision, Project administration, Funding acquisition. All authors have read and approved the final manuscript.

Competing interests

The authors declare no competing interests.

Acknowledgments

This study was supported by the National Natural Science Foundation of China (Grant Nos. 81872888, 81821005, 81673489, and 31871414), the Special Project on Precision Medicine under the National Key R&D Program (Grant No. 2017YFC0906600), the Shanghai Science and Technology Development Funds, China (Grant No. 19JC1416300), the Key New Drug Creation and Manufacturing Program of China (Grant Nos. 2018ZX09711002-004 and 2018ZX09711002-007), and the KC Wong Education Foundation.

Supplementary material

Supplementary data to this article can be found online at https://doi.org/10.1016/j.gpb.2020.09.003.

ORCID

ORCID 0000-0002-7517-4801 (Yuejing Jiang)
ORCID 0000-0002-1290-8134 (Xiaoji Cong)
ORCID 0000-0002-9005-754X (Shangwen Jiang)
ORCID 0000-0002-0608-2815 (Ying Dong)
ORCID 0000-0002-1460-4839 (Lei Zhao)
ORCID 0000-0001-9835-922X (Yi Zang)
ORCID 0000-0002-6784-9653 (Minjia Tan)
ORCID 0000-0003-3224-001X (Jia Li)

References

[1] Acland M, Mittal P, Lokman NA, Klingler-Hoffmann M, Oehler MK, Hoffmann P. Mass spectrometry analyses of multicellular tumor spheroids. Proteomics Clin Appl 2018;12:e1700124.
[2] Mihaylova MM, Shaw RJ. The AMPK signalling pathway coordinates cell growth, autophagy and metabolism. Nat Cell Biol 2011;13:1016–23.
[3] Shaw RJ, Kosmatka M, Bardeesy N, Hurley RL, Witters LA, DePinho RA, et al. The tumor suppressor LKB1 kinase directly activates AMP-activated kinase and regulates apoptosis in response to energy stress. Proc Natl Acad Sci U S A 2004;101:3329–35.
[4] Foretz M, Guigas B, Viollet B. From cancer to diabetes treatment: the tumor suppressor LKB1 as a new pharmacological target. Med Sci 2006;22:348–50.
[5] Shaw RJ, Lamia KA, Vasquez D, Koo SH, Bardeesy N, Depinho RA, et al. The kinase LKB1 mediates glucose homeostasis in liver and therapeutic effects of metformin. Science 2005;310:1642–6.
[6] Zhou G, Myers R, Li Y, Chen Y, Shen X, Fenyk-Melody J, et al. Role of AMP-activated protein kinase in mechanism of metformin action. J Clin Invest 2001;108:1167–74.
[7] Storozhuk Y, Hopmans SN, Sanli T, Barron C, Tsiani E, Cutz JC, et al. Metformin inhibits growth and enhances radiation response of non-small cell lung cancer (NSCLC) through ATM and AMPK. Br J Cancer 2013;108:2021–32.
[8] Sun Y, Tao C, Huang X, He H, Shi H, Zhang Q, et al. Metformin induces apoptosis of human hepatocellular carcinoma HepG2 cells by activating an AMPK/p53/miR-23a/FOXA1 pathway. Onco Targets Ther 2016;9:2845–53.
[9] Zou J, Hong L, Luo C, Li Z, Zhu Y, Huang T, et al. Metformin inhibits estrogen-dependent endometrial cancer cell growth by activating the AMPK-FOXO1 signal pathway. Cancer Sci 2016;107:1806–17.
[10] Zhuang Y, Miskimins WK. Cell cycle arrest in Metformin treated breast cancer cells involves activation of AMPK, downregulation of cyclin D1, and requires p27Kip1 or p21Cip1. J Mol Signal 2008;3:18.
[11] Paiva-Oliveira DI, Martins-Neves SR, Abrunhosa AJ, Fontes-Ribeiro C, Gomes CMF. Therapeutic potential of the metabolic modulator Metformin on osteosarcoma cancer stem-like cells. Cancer Chemother Pharmacol 2018;81:49–63.
[12] Song CW, Lee H, Dings RP, Williams B, Powers J, Santos TD, et al. Metformin kills and radiosensitizes cancer cells and preferentially kills cancer stem cells. Sci Rep 2012;2:362.
[13] Soo JS, Ng CH, Tan SH, Malik RA, Teh YC, Tan BS, et al. Metformin synergizes 5-fluorouracil, epirubicin, and cyclophosphamide (FEC) combination therapy through impairing intracellular ATP production and DNA repair in breast cancer stem cells. Apoptosis 2015;20:1373–87.
[14] Sui X, Xu Y, Yang J, Fang Y, Lou H, Han W, et al. Use of metformin alone is not associated with survival outcomes of colorectal cancer cell but AMPK activator AICAR sensitizes anticancer effect of 5-fluorouracil through AMPK activation. PLoS One 2014;9:e97781.
[15] Zadra G, Batista JL, Loda M. Dissecting the dual role of AMPK in cancer: from experimental to human studies. Mol Cancer Res 2015;13:1059–72.
[16] Egan DF, Shackelford DB, Mihaylova MM, Gelino S, Kohnz RA, Mair W, et al. Phosphorylation of ULK1 (hATG1) by AMP-activated protein kinase connects energy sensing to mitophagy. Science 2011;331:456–61.
[17] Jeon SM, Chandel NS, Hay N. AMPK regulates NADPH homeostasis to promote tumour cell survival during energy stress. Nature 2012;485:661–5.
[18] Choudhury Y, Yang Z, Ahmad I, Nixon C, Salt IP, Leung HY. AMP-activated protein kinase (AMPK) as a potential therapeutic target independent of PI3K/Akt signaling in prostate cancer. Oncoscience 2014;1:446–56.
[19] Muaddi H, Chowdhury S, Vellanki R, Zamiara P, Koritzinsky M. Contributions of AMPK and p53 dependent signaling to radiation response in the presence of metformin. Radiother Oncol 2013;108:446–50.
[20] Zhou G, Wang J, Zhao M, Xie TX, Tanaka N, Sano D, et al. Gain-of-function mutant p53 promotes cell growth and cancer cell metabolism via inhibition of AMPK activation. Mol Cell 2014;54:960–74.
[21] Lee DH, Lee TH, Jung CH, Kim YH. Wogonin induces apoptosis by activating the AMPK and p53 signaling pathways in human glioblastoma cells. Cell Signal 2012;24:2216–25.
[22] Li QR, Yan XM, Guo L, Li J, Zang Y. AMPK regulates anaphase central spindle length by phosphorylation of KIF4A. J Mol Cell Biol 2018;10:2–17.

[23] Visnjic D, Dembitz V, Lalic H. The role of AMPK/mTOR modulators in therapy of acute myeloid leukemia. Curr Med Chem 2019;26:2208–29.
[24] You MK, Kim HJ, Kook JH, Kim HA. St. John's Wort regulates proliferation and apoptosis in MCF-7 human breast cancer cells by inhibiting AMPK/mTOR and activating the mitochondrial pathway. Int J Mol Sci 2018;19:966.
[25] Bungard D, Fuerth BJ, Zeng PY, Faubert B, Maas NL, Viollet B, et al. Signaling kinase AMPK activates stress-promoted transcription via histone H2B phosphorylation. Science 2010;329:1201–5.
[26] Zhang CS, Lin SC. AMPK promotes autophagy by facilitating mitochondrial fission. Cell Metab 2016;23:399–401.
[27] Toyama EQ, Herzig S, Courchet J, Lewis Jr TL, Loson OC, Hellberg K, et al. AMP-activated protein kinase mediates mitochondrial fission in response to energy stress. Science 2016;351:275–81.
[28] Jiang Z, Chen X, Chen K, Sun L, Gao L, Zhou C, et al. YAP inhibition by resveratrol via activation of AMPK enhances the sensitivity of pancreatic cancer cells to gemcitabine. Nutrients 2016;8:546.
[29] Fu X, Wan S, Lyu YL, Liu LF, Qi H. Etoposide induces ATM-dependent mitochondrial biogenesis through AMPK activation. PLoS One 2008;3:e2009.
[30] Luo L, Huang W, Tao R, Hu N, Xiao ZX, Luo Z. ATM and LKB1 dependent activation of AMPK sensitizes cancer cells to etoposide-induced apoptosis. Cancer Lett 2013;328:114–9.
[31] Toulany M, Mihatsch J, Holler M, Chaachouay H, Rodemann HP. Cisplatin-mediated radiosensitization of non-small cell lung cancer cells is stimulated by ATM inhibition. Radiother Oncol 2014;111:228–36.
[32] Negrini S, Gorgoulis VG, Halazonetis TD. Genomic instability–an evolving hallmark of cancer. Nat Rev Mol Cell Biol 2010;11:220–8.
[33] Zannella VE, Cojocari D, Hilgendorf S, Vellanki RN, Chung S, Wouters BG, et al. AMPK regulates metabolism and survival in response to ionizing radiation. Radiother Oncol 2011;99:293–9.
[34] Sanli T, Storozhuk Y, Linher-Melville K, Bristow RG, Laderout K, Viollet B, et al. Ionizing radiation regulates the expression of AMP-activated protein kinase (AMPK) in epithelial cancer cells: modulation of cellular signals regulating cell cycle and survival. Radiother Oncol 2012;102:459–65.
[35] Ui A, Ogiwara H, Nakajima S, Kanno S, Watanabe R, Harata M, et al. Possible involvement of LKB1-AMPK signaling in non-homologous end joining. Oncogene 2014;33:1640–8.
[36] Xin J, Yang H, Fan N, Zhao B, Ouyang Z, Liu Z, et al. Highly efficient generation of GGTA1 biallelic knockout inbred mini-pigs with TALENs. PLoS One 2013;8:e84250.
[37] Ishibashi S, Cliffe R, Amaya E. Highly efficient bi-allelic mutation rates using TALENs in *Xenopus tropicalis*. Biol Open 2012;1:1273–6.
[38] Liu Y, Luo D, Zhao H, Zhu Z, Hu W, Cheng CH. Inheritable and precise large genomic deletions of non-coding RNA genes in zebrafish using TALENs. PLoS One 2013;8:e76387.
[39] Panda SK, Wefers B, Ortiz O, Floss T, Schmid B, Haass C, et al. Highly efficient targeted mutagenesis in mice using TALENs. Genetics 2013;195:703–13.
[40] Katsuyama T, Akmammedov A, Seimiya M, Hess SC, Sievers C, Paro R. An efficient strategy for TALEN-mediated genome engineering in *Drosophila*. Nucleic Acids Res 2013;41:e163.
[41] Wefers B, Panda SK, Ortiz O, Brandl C, Hensler S, Hansen J, et al. Generation of targeted mouse mutants by embryo microinjection of TALEN mRNA. Nat Protoc 2013;8:2355–79.
[42] Ferguson C, McKay M, Harris RA, Homanics GE. Toll-like receptor 4 (Tlr4) knockout rats produced by transcriptional activator-like effector nuclease (TALEN)-mediated gene inactivation. Alcohol 2013;47:595–9.
[43] Ding Q, Lee YK, Schaefer EA, Peters DT, Veres A, Kim K, et al. A TALEN genome-editing system for generating human stem cell-based disease models. Cell Stem Cell 2013;12:238–51.
[44] Fernandez-Capetillo O, Chen HT, Celeste A, Ward I, Romanienko PJ, Morales JC, et al. DNA damage-induced G2-M checkpoint activation by histone H2AX and 53BP1. Nat Cell Biol 2002;4:993–7.
[45] Deckbar D, Jeggo PA, Lobrich M. Understanding the limitations of radiation-induced cell cycle checkpoints. Crit Rev Biochem Mol Biol 2011;46:271–83.
[46] Ruprecht B, Roesli C, Lemeer S, Kuster B. MALDI-TOF and nESI Orbitrap MS/MS identify orthogonal parts of the phosphoproteome. Proteomics 2016;16:1447–56.
[47] Wickramasinghe VO, Venkitaraman AR. RNA processing and genome stability: cause and consequence. Mol Cell 2016;61:496–505.
[48] Hardie DG, Schaffer BE, Brunet A. AMPK: an energy-sensing pathway with multiple inputs and outputs. Trends Cell Biol 2016;26:190–201.
[49] Bergamaschi D, Samuels Y, Jin B, Duraisingham S, Crook T, Lu X. ASPP1 and ASPP2: common activators of p53 family members. Mol Cell Biol 2004;24:1341–50.
[50] Slee EA, Lu X. The ASPP family: deciding between life and death after DNA damage. Toxicol Lett 2003;139:81–7.
[51] Huang X, Yan J, Zhang M, Wang Y, Chen Y, Fu X, et al. Targeting epigenetic crosstalk as a therapeutic strategy for EZH2-aberrant solid tumors. Cell 2018;175:186–99.e19.
[52] Nakaoka S, Sasaki K, Ito A, Nakao Y, Yoshida M. A genetically encoded FRET probe to detect intranucleosomal histone H3K9 or H3K14 acetylation using BRD4, a BET family member. ACS Chem Biol 2016;11:729–33.
[53] Liu Y, Wang X, Zhang J, Huang H, Ding B, Wu J, et al. Structural basis and binding properties of the second bromodomain of Brd4 with acetylated histone tails. Biochemistry 2008;47:6403–17.
[54] Filippakopoulos P, Picaud S, Mangos M, Keates T, Lambert JP, Barsyte-Lovejoy D, et al. Histone recognition and large-scale structural analysis of the human bromodomain family. Cell 2012;149:214–31.
[55] Choi S, Bakkenist CJ. Brd4 shields chromatin from ATM kinase signaling storms. Sci Signal 2013;6:pe30.
[56] Zhang C, Su ZY, Wang L, Shu L, Yang Y, Guo Y, et al. Epigenetic blockade of neoplastic transformation by bromodomain and extra-terminal (BET) domain protein inhibitor JQ-1. Biochem Pharmacol 2016;117:35–45.
[57] Stewart HJ, Horne GA, Bastow S, Chevassut TJ. BRD4 associates with p53 in DNMT3A-mutated leukemia cells and is implicated in apoptosis by the bromodomain inhibitor JQ1. Cancer Med 2013;2:826–35.
[58] Dey A, Chitsaz F, Abbasi A, Misteli T, Ozato K. The double bromodomain protein Brd4 binds to acetylated chromatin during interphase and mitosis. Proc Natl Acad Sci U S A 2003;100:8758–63.
[59] Katajisto P, Vallenius T, Vaahtomeri K, Ekman N, Udd L, Tiainen M, et al. The LKB1 tumor suppressor kinase in human disease. Biochim Biophys Acta 2007;1775:63–75.
[60] Kim J, Kundu M, Viollet B, Guan KL. AMPK and mTOR regulate autophagy through direct phosphorylation of Ulk1. Nat Cell Biol 2011;13:132–41.
[61] van Veelen W, Korsse SE, van de Laar L, Peppelenbosch MP. The long and winding road to rational treatment of cancer associated with LKB1/AMPK/TSC/mTORC1 signaling. Oncogene 2011;30:2289–303.
[62] Howell JJ, Hellberg K, Turner M, Talbott G, Kolar MJ, Ross DS, et al. Metformin inhibits hepatic mTORC1 signaling via dose-dependent mechanisms involving AMPK and the TSC complex. Cell Metab 2017;25:463–71.

[63] Inoki K, Kim J, Guan KL. AMPK and mTOR in cellular energy homeostasis and drug targets. Annu Rev Pharmacol Toxicol 2012;52:381–400.
[64] Whiteside TL. The tumor microenvironment and its role in promoting tumor growth. Oncogene 2008;27:5904–12.
[65] Heidegger I, Pircher A, Pichler R. Targeting the tumor microenvironment in renal cell cancer biology and therapy. Front Oncol 2019;9:490.
[66] Hanahan D, Weinberg RA. Hallmarks of cancer: the next generation. Cell 2011;144:646–74.
[67] Reynolds TY, Rockwell S, Glazer PM. Genetic instability induced by the tumor microenvironment. Cancer Res 1996;56:5754–7.
[68] Xu H, Zhou Y, Coughlan KA, Ding Y, Wang S, Wu Y, et al. AMPKalpha1 deficiency promotes cellular proliferation and DNA damage via p21 reduction in mouse embryonic fibroblasts. Biochim Biophys Acta 2015;1853:65–73.
[69] Rashid A, Liu C, Sanli T, Tsiani E, Singh G, Bristow RG, et al. Resveratrol enhances prostate cancer cell response to ionizing radiation. Modulation of the AMPK, Akt and mTOR pathways. Radiat Oncol 2011;6:144.
[70] Samuels-Lev Y, O'Connor DJ, Bergamaschi D, Trigiante G, Hsieh JK, Zhong S, et al. ASPP proteins specifically stimulate the apoptotic function of p53. Mol Cell 2001;8:781–94.
[71] Vives V, Su J, Zhong S, Ratnayaka I, Slee E, Goldin R, et al. ASPP2 is a haploinsufficient tumor suppressor that cooperates with p53 to suppress tumor growth. Genes Dev 2006;20:1262–7.
[72] Mori T, Okamoto H, Takahashi N, Ueda R, Okamoto T. Aberrant overexpression of 53BP2 mRNA in lung cancer cell lines. FEBS Lett 2000;465:124–8.
[73] Ao Y, Rohde LH, Naumovski L. p53-interacting protein 53BP2 inhibits clonogenic survival and sensitizes cells to doxorubicin but not paclitaxel-induced apoptosis. Oncogene 2001;20:2720–5.
[74] Nie L, Shuai L, Zhu M, Liu P, Xie ZF, Jiang S, et al. The landscape of histone modifications in a high-fat diet-induced obese (DIO) mouse model. Mol Cell Proteomics 2017;16:1324–34.
[75] Shechter D, Dormann HL, Allis CD, Hake SB. Extraction, purification and analysis of histones. Nat Protoc 2007;2:1445–57.